PRELIMINARY STRUCTURAL DESIGN OF A HIGH ASPECT RATIO TRANSPORT AIRCRAFT WITH LAMINAR WING

Markus R. Ritter[1], Martin Schmalz[1] & Michael Fehrs[1]

[1]Institute of Aeroelasticity, German Aerospace Center (DLR), Göttingen, Germany

Abstract

A high aspect ratio jet transport aircraft with a laminar wing is designed within the project *ULTIMATE* funded by the German Federal Aeronautical Research Programme. The design of the wing features both a high aspect ratio (> 15) as well as a laminar airfoil layout with natural laminar flow (NLF) realized by a particular leading edge shape to obtain Crossflow Attenuated Natural Laminar Flow (CATNLF) in the inner region of the wing. A particular challenge is the structural design and optimization of this wing due to the impact of static and dynamic aerodynamic and aeroelastic effects, which must be considered throughout the whole design process. In this work we present an approach for the generation and assessment of the structural model based on aeroelastic models of mixed fidelity (potential aerodynamics as well as CFD) which are derived from a prescribed aerodynamic (flight) shape of the wing. For the structural optimization of the wing, load cases requested by the CS-25 specifications (including steady and quasi-steady maneuver as well as gust loads) are considered and five different mass cases, ranging from empty to maximum take-off mass are used. Steady CFD RANS simulations with free transition modeling are performed for cruise flight conditions to assess the impact of elastic structural deformations caused by different fuel or payload fractions on the performance of the laminar wing. The results reveal that the laminar wing is very robust against elastic structural deformations during cruise flight for the mass cases considered.

Keywords: High Aspect Ratio Wing, Natural Laminar Flow, CATNLF, DLR F25

1. Background and Motivation

As specified by Breguet's range equation, the fuel consumption and thus the CO2 emissions of an aircraft can be reduced basically by two parameters. On the one hand, by reducing the mass of the aircraft, and, on the other, by improving its aerodynamic efficiency. The wing design, and especially the airfoil is of central importance for the performance and thus the efficiency of the aircraft. Significant improvements of the aerodynamic performance can be achieved both by increasing the aspect ratio to lower the induced drag and by maximizing the portion of laminar flow around the wing. In order to avoid a disproportionate increase in wing mass due to the high aspect ratio, actively controlled load reduction and flutter suppression systems might become necessary. This requires a highly integrated design process with simultaneous consideration of control surfaces, systems, flight control, structural concepts, aerodynamics and aeroelasticity as well as sensor technology [1]. Attention must be paid to enable a cruise speed of the aircraft equipped with the NLF wing which is close to the cruise speed of a conventional, i.e. turbulent wing design of comparable size and mission [5]. The design of such an aircraft with both a high aspect ratio wing (HARW) as well as a NLF design is the goal of the project *ULTIMATE* funded by the German Federal Aeronautical Research Programme. The aircraft investigated itself is a derivate of the DLR F25 configuration, which features a similar layout but uses a classical turbulent wing design [2]. A number of wind tunnel tests in the European Transonic Windtunnel (ETW) companion the numerical design of the wing at transonic flight speeds and realistic Reynolds numbers.

Realizing long regions of natural laminar flow (NLF) at high subsonic flight speeds to obtain a significant reduction of surface friction drag at a mid-range jet transport is a challenging task. A new NLF technology, the Crossflow Attenuated NLF (CATNLF), which was developed in the past years, uses a particular shaping of the wing's geometry (especially the leading edge) to produce a surface pressure distribution that delays boundary layer transition due to crossflow [3, 4, 5]. The basic idea is the very strong acceleration of the flow around the leading edge to control (avoid) cross-flow transition, and, from the region of the leading edge to approximately 60% of the chord of the airfoil, keep a favorable but very flat pressure gradient followed by the beginning of the transition region which is close to the compression shock. In addition, the leading edge sweep angle can be increased which is beneficial in terms of a higher Mach number. The aerodynamic design of the wing of the aircraft investigated in this work was done in a cooperation with Airbus Operations and is detailed in the work of Streit [6]. An extensive numerical design and test procedure based on a combination of full potential and CFD methods including compressible boundary layer solutions was conducted to optimize the outer shape of the wing of the aircraft. As a result, the planform and the airfoils of the wing were fixed to a moderate sweep angle, and the design (cruise) Mach number was set to 0.77 which corresponds to case C in [6]. Following the design of the wing and the airfoils, the complete DLR HARW aircraft was build in a CAD program. The horizontal and vertical tail planes as well as the fuselage were adopted from the baseline DLR F25 configuration, which features a similar design, but with a classical (turbulent) wing layout with a slightly higher leading edge sweep angle [2]. Figure 1 shows the aircraft. This configuration features a high aspect ratio wing for significant reduction of the induced drag. The high aspect ratio complicates the wing design, however, because the local lift coefficient takes comparatively large values due to the taper of the wing, which is a problem for high subsonic and transonic flows. It should be mentioned that particular high lift devices are necessary to ensure a smooth upper surface of the wing without steps or protruding edges as is the case if classical leading edge slats or droop flaps are used. This will be realized by the application of Krüger flaps which are installed on the lower side of the wing, thus leaving the upper surface clean. On the other hand, this restricts the laminar flow region to the upper side of the wing.

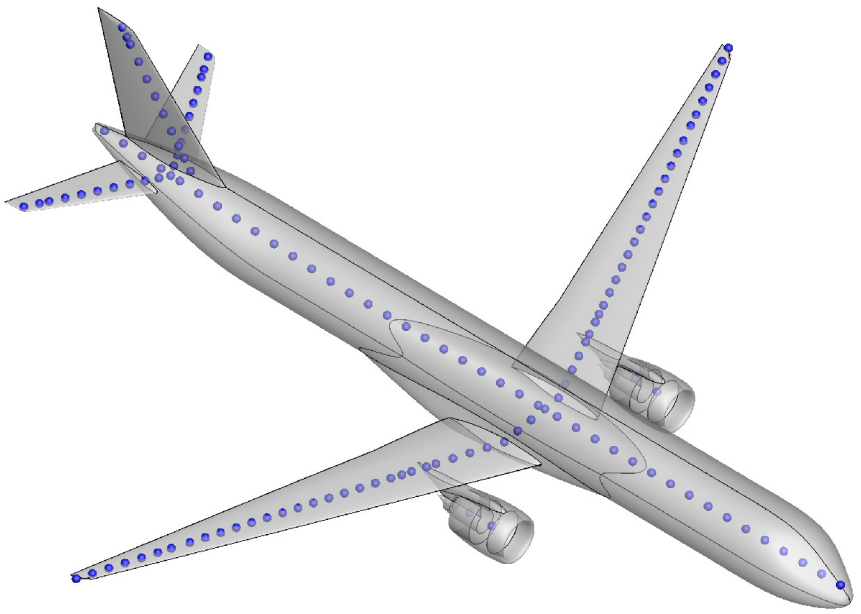

Figure 1 – Outer shape of the HARW aircraft configuration. The aspect ratio is above 15. Blue dots illustrate the nodes of the loads reference axis of the corresponding structural model.

An exemplary airfoil section at an inner station of the wing is plotted in Figure 2. It reveals the distinctive kink at the leading edge of the airfoil, which is required for the strong acceleration of the flow. Table 1 lists selected Top Level Aircraft Requirements (TLARs) of this configuration.

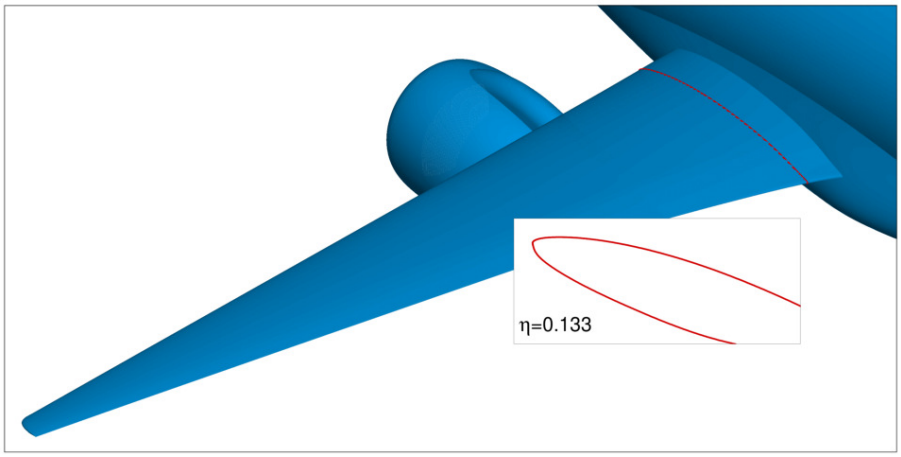

Figure 2 – Airfoil section with the distinctive kink at the leading edge for strong flow acceleration in the inner region near the root.

Table 1 – Top Level Aircraft Requirements of the DLR HARW aircraft.

Property	Unit	Value
Design Range	nm	2500
Design PAX (single class)	-	239
Mass per PAX	kg	95
Design Payload	kg	25000
Max. Payload	kg	25000
Design Cruise Mach number (MC) [6]	-	0.77
Design Flight Level (FL) [6]	-	350

The aerodynamic design of the CATNLF wing is a complex task which is primarily focused on optimal performance at the design point; however, also off-design characteristics must be considered to a certain extent [6]. Fuel burn during the mission reduces the mass of the aircraft, and to stay close to the (aerodynamic) design point the flight altitude is typically varied (increased). In addition, the wing of the HARW aircraft is characterized by a high flexibility because of the high aspect ratio. Considering the fuel, which is entirely stored in the main wings, the question arises how the elastic structural deformations of the wing – as the result of varying fuel or payload mass – impact the behavior of the laminar wing. The structural stiffness of the wing is not a design goal but a result of the structural optimization process, for which a number of load cases according to EASA CS-25 certification specifications [17] as well as constraints for the material strains (composite materials are used for the primary structure of the aircraft) are considered [8, 7, 9, 10, 2]. This is the usual approach for the structural optimization of short- and medium-range jet transport aircraft. Aeroelastic constraints are typically set to ensure a particular control surface efficiency (mainly for the ailerons) , but not to confine e.g. the twist deformation of the wing in order to improve aerodynamic performance as the wing changes its shape due to fuel burn during flight or due to different amounts of payload. Hence it would be possible to increase the stiffness of the wing to keep the aerodynamic properties of the laminar wing over the entire mission at the cost of additional structural mass, i.e. a tradeoff exists between aerodynamic performance on the one hand and structural mass on the other. To make a decision in this regard, the sensitivity of the aerodynamic characteristics (drag) of the laminar wing as function of elastic structural deformation of the wing (in twist and bending) must be computed, which is one of the goals of this work. Based on this sensitivity, a decision can be made whether additional constraints are meaningful for the structural optimization of the wing to increase its stiffness properties.

2. Loads Analyses and Structural Optimization

This section details the setup and the optimization of the structural model of the DLR HARW aircraft. Various topological parameters of the inner structure of the aircraft were already defined in the conceptual design phase. These include the location of the spars, the ribs, and the stringers of the main wing and the tail surfaces. For the structural optimization of the aircraft, a set of aeroelastic simulation models including an aerodynamic model, a stiffness model and several mass models are built [8, 7, 9]. These models are generated by an automated parametric process chain based on an adapted Common Parametric Aircraft Configuration Schema (CPACS) data file of the DLR F25, which features similar layout, geometry, and aircraft configuration as the HARW aircraft of this work [2]. CPACS describes a wide range of aircraft characteristics including the outer geometry (profiles and segments), the global aircraft parameters, the topology of the inner structure (e.g. locations of ribs, spars, and stringers), the engine outer geometry, and many more [12, 13]. Particular aircraft information, processed information like aerodynamic data, aircraft loads, and detailed mass distributions for each component, together with tool parameters, can be stored as well in the CPACS dataset. Starting from the fixed aerodynamic outer surface, i.e. the wing of the DLR HARW aircraft in flight shape as designed by Streit et al. [6], the aeroelastic model of the aircraft for the optimization of the primary structure is built by the automated in-house parametric model generator cpacs-MONA, which has been derived from the basic MONA process at DLR-AE to perform aeroelastic structural design for various aircraft configurations for the preliminary design using physics-based simulations [8, 7, 9, 10, 2]. cpacs-MONA is integrated in various design processes and high-fidelity multi-disciplinary-optimization (MDO) chains at DLR [11]. It can also be used as a stand-alone tool, as was done for this work. cpacs-MONA reads the information about the wing planform, the wing topology – like ribs and spar positions – the stringer pitch and initial component thicknesses together with the engine, pylon, and landing gear. It also uses information about aircraft masses such as design, primary and secondary masses plus the dimensions of the control surfaces, as well as the fuel tanks. With this information, cpacs-MONA creates input-files for the involved tools. The finite element (FE) models for MSC Nastran of the individual aircraft components (wing, horizontal and vertical tail, fuselage) are build by ModGen, a parametric FE model generator, separately. All components are then combined to the global FE model (GFEM). The GFEM includes the primary and secondary structural masses (plus trim masses and fuel) and can thus be used for dynamic analyses. cpacs-MONA combines several tools written in different programming languages forming an automated process flow as highlighted in Figure 3. The process starts with an estimation of preliminary loads based on conceptual design methods followed by an estimation of a generic beam model representing the fuselage stiffness[14]. The conceptual loads are used for a preliminary cross-section sizing (PCS) within ModGen [15]. Due to the PCS, a more realistic wing representative with respect to the shell thickness distribution and bar properties is provided. As shown in Figure 4, the wing ribs, spars, and skins are modeled with shell elements. The other wing component structures like the spar caps, the inner reinforcement structure, or the stringers are modeled with bar or beam elements. A parametric elastic pylon model is also available to account for the interaction of the engine with the wing and vice versa. For a comprehensive aeroelastic analysis, reasonable mass models have to be set up. Therefore, a mass model tool reads the mass-breakdown for each component and creates a model with distributed mass and inertia entities in line with the given geometrical space of the individual component. The fuel tank volume is calculated according to the geometrical borders (ribs, spars) as defined in CPACS. The masses of the engine and landing gear are extracted from the CPACS dataset and converted into Nastran *CONM2* discrete mass elements. The resulting operating mass empty (OME) together with defined combinations of fuel and payload/passenger masses form the design masses and different mass cases important for the loads analysis of the aircraft. To reduce the complexity of the GFEM for the extensive loads analysis, the stiffness of the structural model is condensed to the loads reference axis (LRA) points by a static (Guyan) condensation [16].

The material of the primary structure is a fiber composite with a particular stacking sequence, the laminates includes layers with orientations of 0°, 90°, as well as +45° and -45°. Only the thickness of the entire laminate was used as design variable for the structural optimization, i.e. no lamination parameters were considered. The aeroelastic models are used to calculate a number of steady

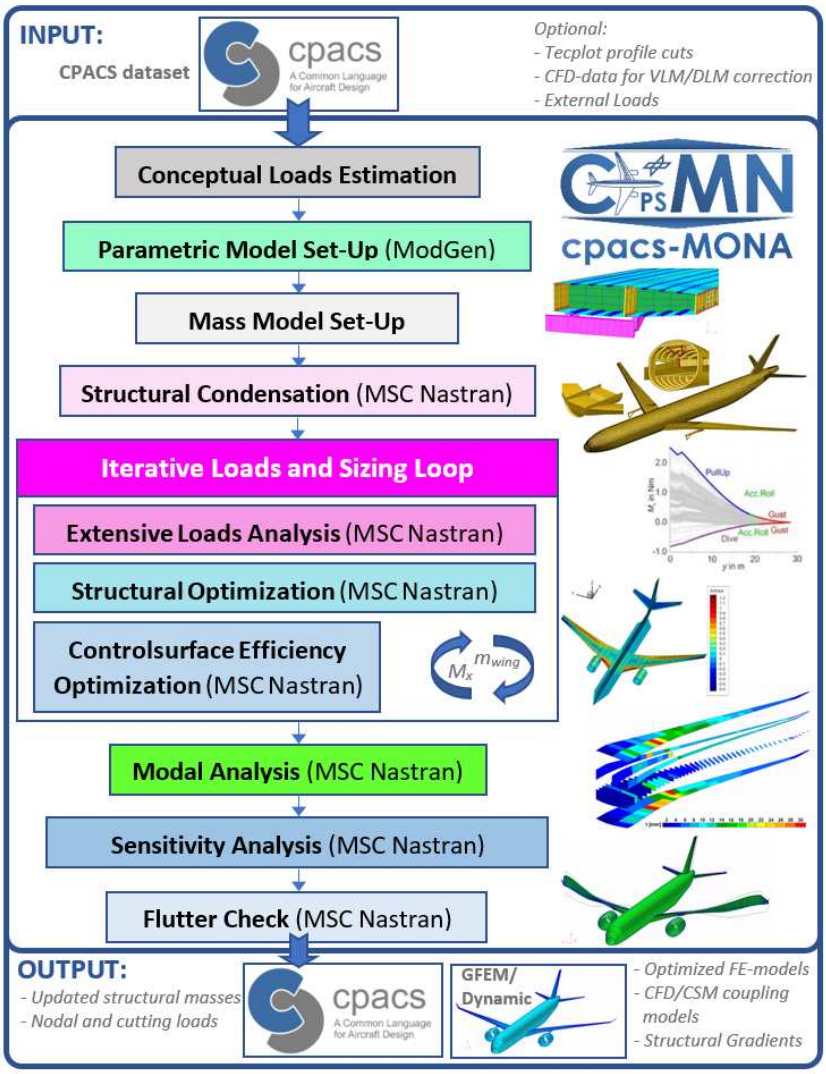

Figure 3 – cpacs-MONA process overview.

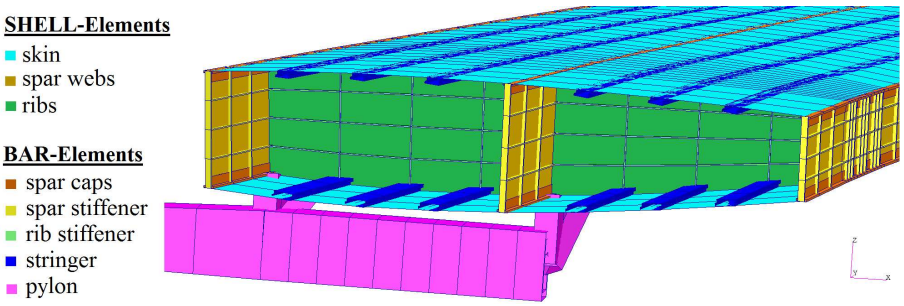

Figure 4 – Topology of the wing FE model component generated by ModGen highlighting the applied structural elements.

and quasi-steady (-1g, 1g, and 2.5g), as well as dynamic gust loads (discrete 1-cos gusts) at specific flight speeds and five different mass cases (ranging from empty mass up to maximum takeoff mass) with MSC Nastran. The structural design speeds (e.g. VS, VA, VC, VD) and other relevant parameters (e.g. gust gradients) are derived from the CS-25 specifications [17] and particular aircraft parameters. The loads are collected at several monitoring stations along the wing, and a convex hull method is used to select the dimensioning loads that are used for the structural optimization, which is done by MSC Nastran solution sequence SOL200. The loads process implemented in cpacs-MONA is sketched in Figure 5. The entire structural optimization process is repeated several times to account for updates in the structural stiffness and mass distributions of the aircraft until a prescribed

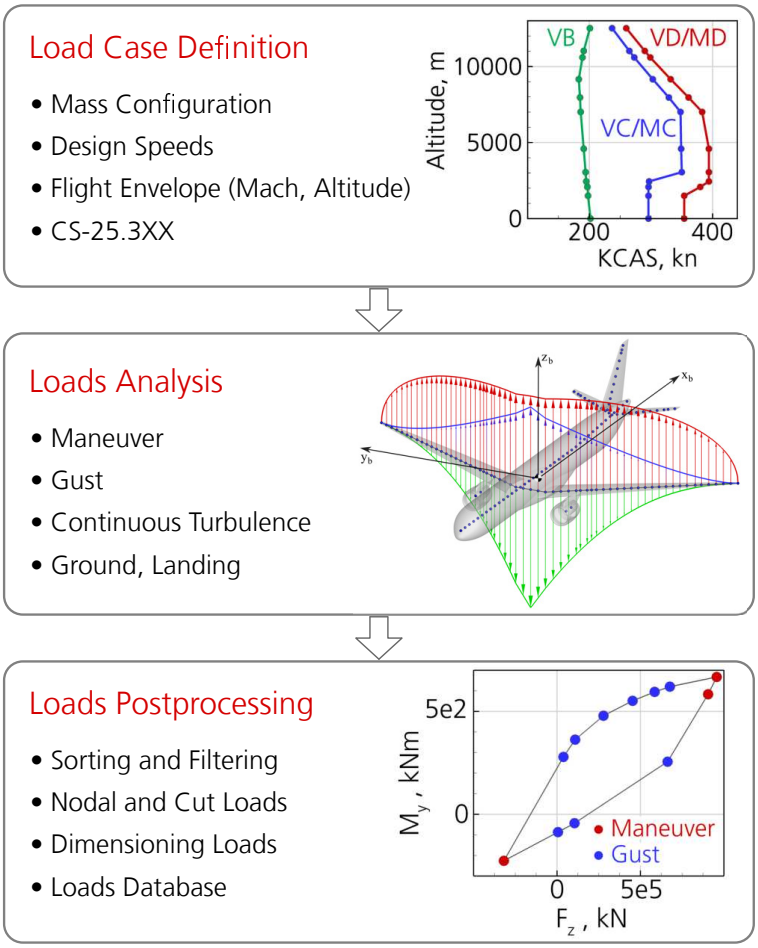

Figure 5 – General loads process as implemented in cpacs-MONA.

criterion (residual) is reached, mostly the change of the mass of the wingbox and other components is monitored. Aeroelastic constraints are imposed for the optimization to ensure sufficient control surface authority, mainly with respect to the ailerons. For the DLR HARW aircraft, five mass cases have been defined and used for the loads and optimization loops. These include Operational Empty Weight (OEW), an intermediate mass case with zero payload and 100% fuel (labeled MFOeF), the Maximum Zero Fuel Weight (MZFW), a cruise mass case with 100% payload and 26% fuel, and the Maximum Take-Off Weight (MTOW). These mass cases are listed in Table 2, where the mass case ID refers to a description of the mass case used by cpacs-MONA. The structural design speeds are

Table 2 – Mass cases used for loads and optimization with payload and fuel fractions.

Mass case ID	MOOee	MFOeF	MZOAe	MCRUI	MTOAa
Design mass case	OEW	-	MZFW	-	MTOW
Payload, %	0	0	100	100	100
Fuel, %	0	100	0	26	49

defined by CS 25.335 specifications [17]. For the DLR HARW aircraft, the equivalent airspeed (EAS), true airspeed (TAS), the Mach number, as well as the dynamic pressure as function of the altitude are plotted in Figure 6. The maximum operating Mach number (MMO) as well as the maximum operating limit speed (VMO) are taken from the conceptual design. For the structural optimization, both quasi-steady maneuver and unsteady gust load cases have been taken into account according to the CS-25 specifications. All loads are computed by MSC Nastran within cpacs-MONA, a reduced structural model derived from a Guyan transformation (cf. the nodes of the loads reference axis in

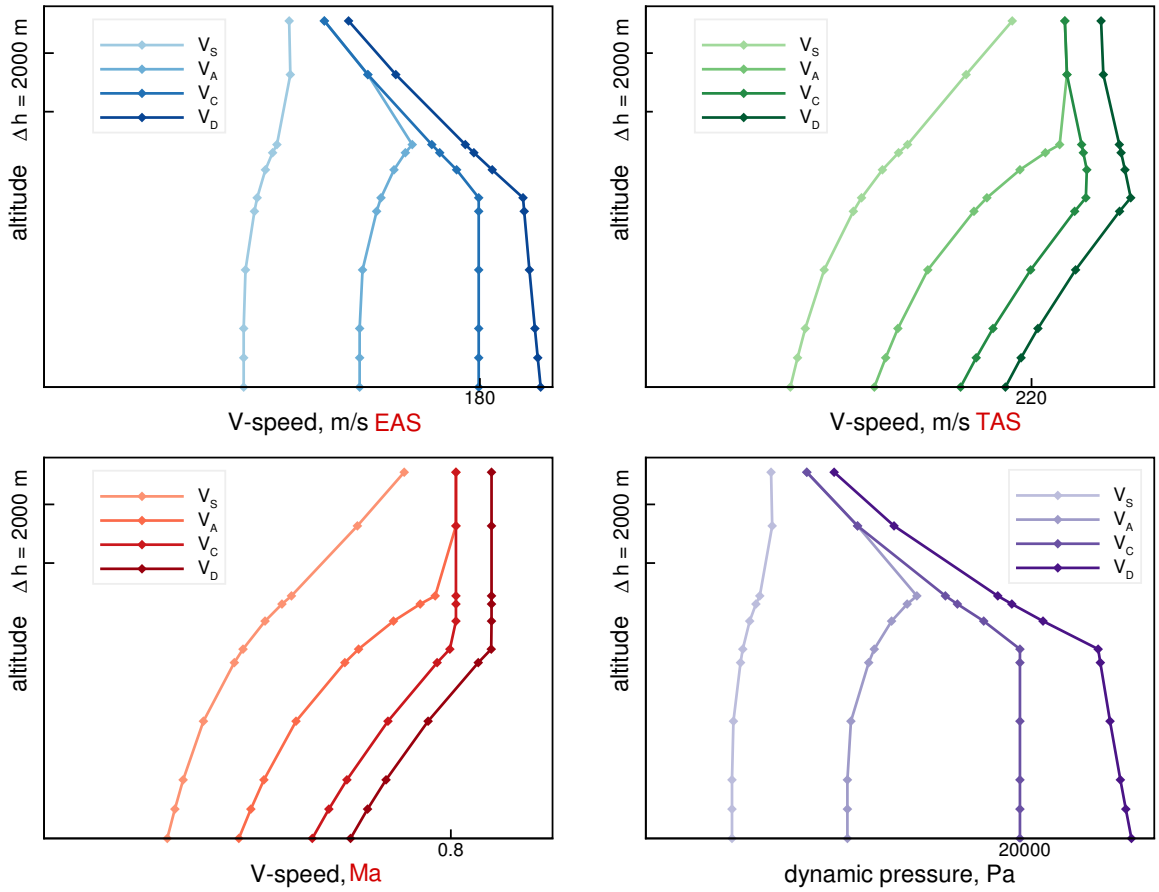

Figure 6 – Structural design airspeeds of the DLR HARW aircraft as function of altitude derived from CS-25 specifications.

Figure 1) is used to reduce the computational effort (only the structural optimization is done with the detailed (GFEM) finite element model). The aeroelastic models are used for the calculation of steady and quasi-steady maneuver loads with prescribed load factors (-1g, 2.5g) by Nastran solution sequence 144, which is based on the vortex-lattice method. Unsteady gust loads are calculated by Nastran solution sequence 146, which uses the doublet-lattice method. A total of 66 load cases are computed with different combinations of mass cases, altitudes, gust gradients, airspeeds, and Mach numbers by cpacs-MONA.

As an example, the torsion and bending moment cut loads from steady and unsteady load cases and the five different mass cases at the inner monitoring station on the right wing are plotted in Figure 7. Also, the convex hull of these loads is shown. As is typical for jet transport aircraft, 2.5g pull-up (maximum My and Mx), -1g push-down (minimum Mx and My) and gust load cases (maximum Mx) constitute the dimensioning load cases. Six monitor stations are used along the wing for the selection of the dimensioning shear and moment loads. The load cases that emerged as dimensioning load cases at the end of the iterative sizing process for the wing are listed in Table 3 together with selected parameters of the loads analyses. As expected and typical for mid-range jet transports, a combination of -1g, 2.5g, and gust load cases at high Mach numbers and high dynamic pressures form the major part of the dimensioning load cases.

Three iterative loads and structural optimization loops were required by cpacs-MONA to reach a convergent solution in terms of the primary structural mass of the aircraft (OEW). The objective for the optimization was the minimum mass of the structure. It was verified that the final model shows no buckling for the maneuver load cases, i.e. the buckling factor as computed by a linear buckling analysis with MSC Nastran is larger than unity. The global structural finite element model (GFEM) is shown together with the material thickness distribution of the finite elements as the result of the structural optimization loops in Figure 8. A minimum thickness of 2 mm was set as lower bound

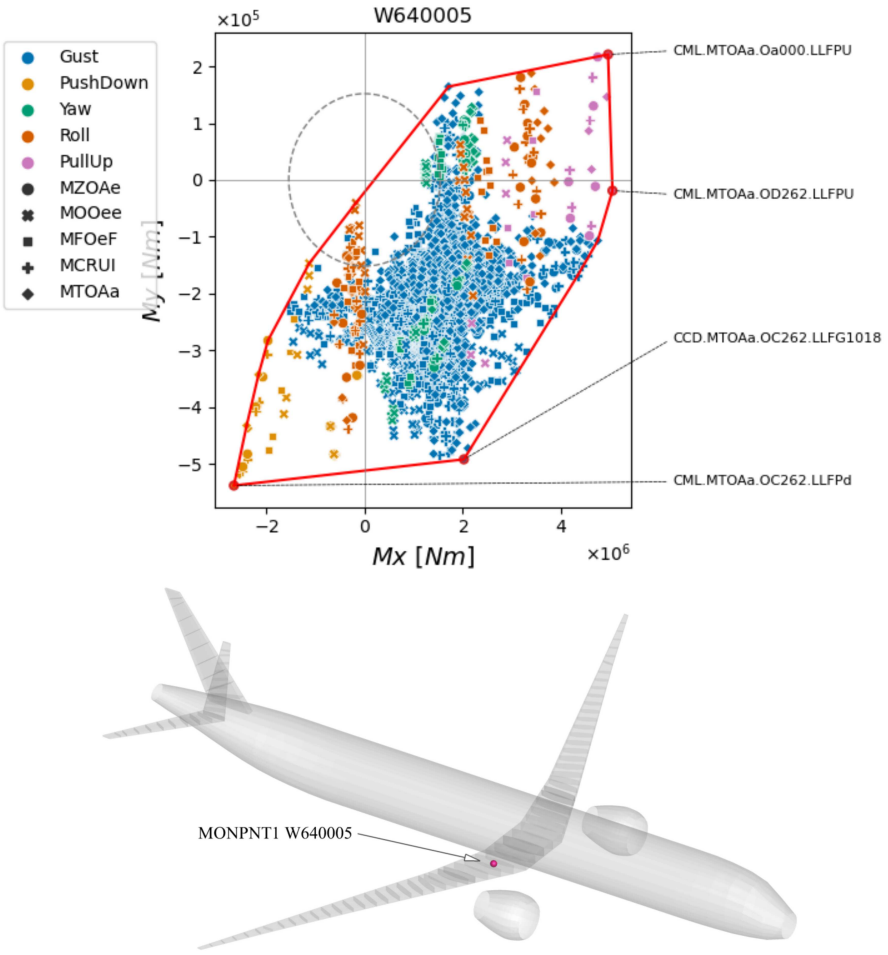

Figure 7 – Torsion (My) and bending moment (Mx) cut loads from steady and unsteady load cases (colors) and five different mass cases (symbols) resolved in a local coordinate system at inner monitoring station on the right wing.

Table 3 – Dimensioning load cases of the DLR HARW aircraft wing with selected parameters.

Mass case ID	load type	structural design speed	altitude, m
MFOeF	Gust	VC	8000
MOOee	Gust	VC	8000
MTOAa	Gust	VC	8000
MTOAa	Gust	VC	8000
MZOAe	Gust	VC	8000
MZOAe	Pull-up, 2.5g	Va	0
MCRUI	Push-down, -1g	VD	8000
MTOAa	Pull-up, 2.5g	Va	0
MTOAa	Pull-up, 2.5g	VD	8000
MTOAa	Push-down, -1g	VC	8000

for the design variables for all elements. Subsequent to the structural optimization process, the jig-bend shape of the model is calculated. Therefore, the cruise mass case (MCRUI) is used and the elastic structural deflections (bending and twist) in 1g steady straight level flight at the cruise Mach number (0.77) are calculated. The bending component of the elastic deformations is scaled, and

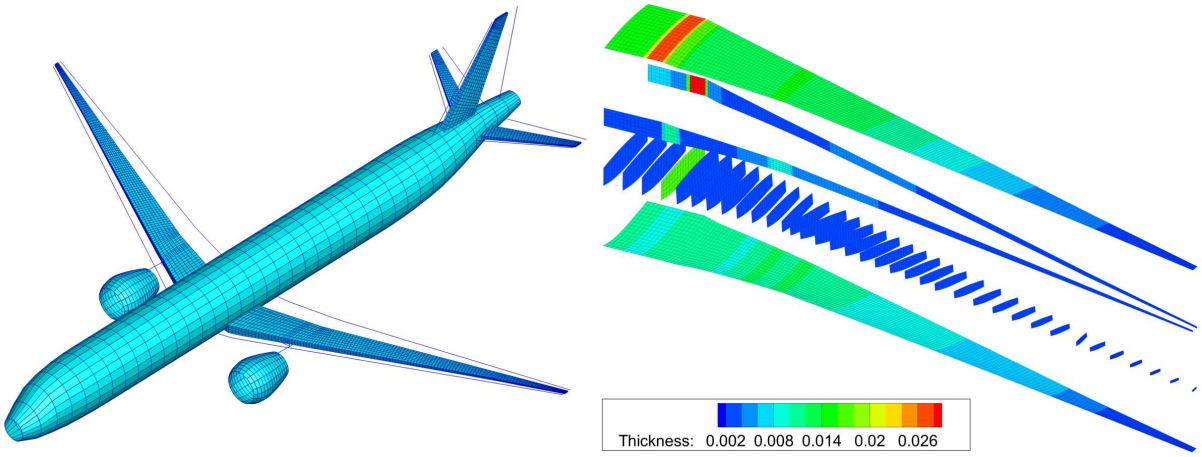

Figure 8 – Detailed finite element model (GFEM) of the DLR HARW aircraft used for structural optimization (left). Material thickness distribution of right wing as the result of structural optimization (right).

taken, together with the twist deformation, to deform the original shape of the wing, such that the resulting model is both in jig-twist and jig-bend shape. It has to be mentioned that the main difference between jig and flight shape is mainly in the twist distribution.
Only a single aeroelastic constraint was set to ensure positive aileron effectiveness throughout the flight envelope. All other constraints are with respect to material strains. Thus the stiffness properties of the final finite element model of the DLR HARW aircraft are the result of the structural optimization process, i.e. the stiffness of the structure or of components was neither part of the objective function nor a constraint. As mentioned in the previous section, one of the goals of this work is to investigate the sensitivity of the laminar wing to elastic structural deformations caused by either different payload or fuel fractions or due to fuel burn during the flight mission. To compute this sensitivity (the exact approach is based on CFD analyses and detailed in the following section), the structural deflections of the aircraft in trimmed 1g steady straight horizontal flight are computed for the four mass cases MOOee, MCRUI, MZOAe, and MTOAa by MSC Nastran solution sequence 144. Each of them uses the same Mach number and the same dynamic pressure which corresponds to the design cruise flight point of the aircraft (Mach number of 0.77, flight level 350 [5]). The corresponding elastic structural deflections provide an estimate of the flexibility of the wing. The elastic deflections of the nodes of the loads reference axis of the right wing in terms of displacements in the z direction as well as rotations about the (global) y axis (twist) are plotted in Figure 9. The elastic rotations about the y axis

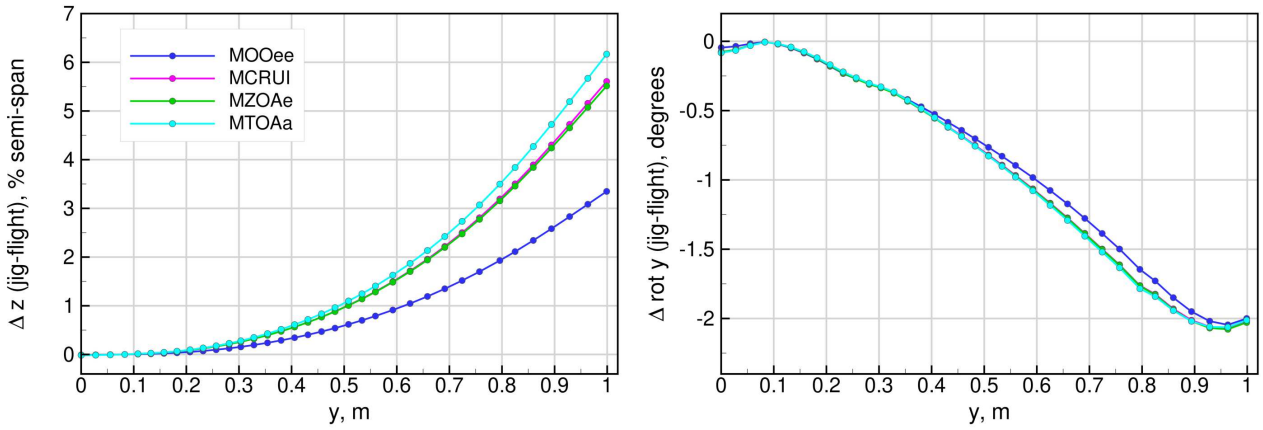

Figure 9 – Elastic structural deflections (deltas from jig to flight) of the loads reference axis nodes in the z direction as well as rotations about the (global) y axis of the right wing of the DLR HARW aircraft for four mass cases in 1g steady straight horizontal flight.

(resolved in the global coordinate system) are almost equal between the four mass cases, despite the fact that the bending deformations differ significantly. This is because two opposing effects might have neutralized each other. On the one hand, for the heavy mass configurations, the angle of attack is higher, and more lift due to angle of attack (roughly at 25% chord) causes more nose-up torsion moment. On the other hand, with larger wing bending deformations, the bending-torsion coupling twists the wing tip nose-down (as seen in the global coordinate system). The maximum structural deflection of approximately 6% (with respect to the semi-span of the wing) in steady straight horizontal flight is obtained for the MTOAa (MTOW) mass case. The deformations are used for the CFD analyses to assess the impact of the structural deflections on the performance (aerodynamic lift and drag) of the laminar wing, as depicted in the following section.

3. CFD Performance Analyses for different Wing Shapes

In this section the sensitivity of the laminar wing of the aircraft to changes in the shape of the wing is computed by steady RANS CFD analyses with free transition modeling. The four shapes of the wing corresponding to the four mass cases (each in 1g steady straight horizontal flight) which were presented in the previous section are used to deform the CFD grid. To this end, a radial basis function method is used to interpolate the deformations of the aeroelastic models onto the CFD surface grid, followed by a deformation of the CFD volume grid. Because the elastic structural displacements are computed for the nodes of the loads references axis (as depicted in Figure 1), a particular method is required to enable a smooth deformation of the CFD grid points. A couplingmodel, as shown in Figure 10, is used for this purpose. The nodes of the loads reference axis are connected to

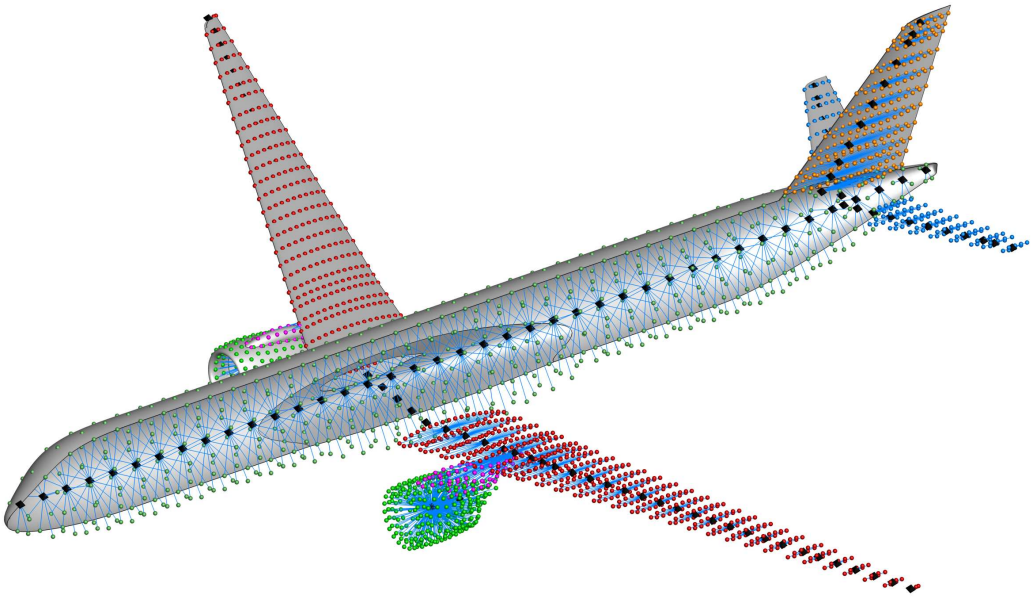

Figure 10 – Couplingmodel for the transfer of structural displacements and rotations of the nodes of the loads reference axis (black markers) on particular points (*couplingpoints*) located at the outer surface of the aircraft by rigid MPC elements.

couplingpoints, which are located at the outer surface (CFD surface grid) of the aircraft, by rigid MPC (MSC Nastran RBE2) elements. The interpolation matrix interpolates the displacements of the couplingpoints to the surrounding CFD grid points. To enable a meaningful comparison of the performance (lift over drag) among the different mass cases, the angles of attack of the aircraft were each iterated in the steady CFD simulations to obtain the same (design) lift coefficient at a Mach number of 0.77 and a flight level of 350, which corresponds to an altitude of approximately 10650 m. No fluid structure coupling was used, all CFD simulations were made with a rigid wing.

The DLR TAU-Code is used for the steady RANS simulations [18]. The TAU transition prediction module [20, 21] is used for transition prediction based on an e^N method [23, 22] in combination with the Menter k-ω SST turbulence model. The transition prediction method is based on the compressible boundary layer code COCO to determine the velocity profiles as input for a local linear stability code

at 24 spanwise locations [19]. The transition location is found at the chordwise location, at which the incompressible N factors exceed either the critical value for Tollmien-Schlichting ($N_{crit,TS} = 12$) or for crossflow transition ($N_{crit,CF} = 9$). Based on theses transition locations, grid points in the laminar boundary layer are identified and the turbulence production in this region is disabled to obtain a laminar boundary layer flow. The CFD grid used for the analyses presented in the following is a half model with a symmetry plane and has approximately 18.7 million nodes.
Figure 11 shows the distribution of the skin friction coefficient on the upper surface of the wing for the original flight shape. It is characterized by long extends of laminar flow along the span from root

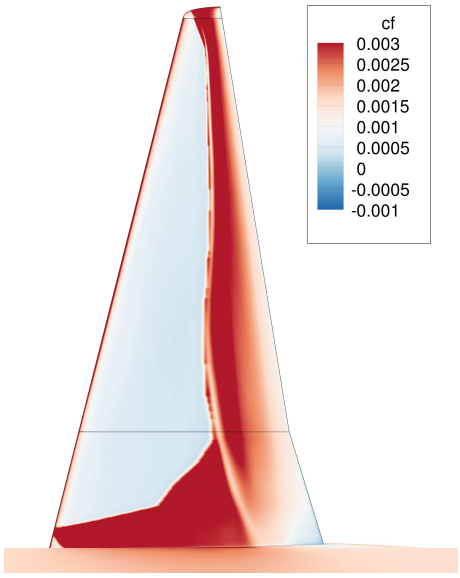

Figure 11 – Skin friction coefficient on the upper surface of the right wing of the DLR HARW aircraft for the original (design) flight shape as predicted by steady RANS simulation with free transition modeling.

to tip. The airfoils were designed for a pressure distribution which is characterized by a favorable pressure gradient between the leading edge and the shock. For the flight shape the beginning of the transition region is at the shock. Figure 12 shows the skin friction coefficient of the right wing of the DLR HARW aircraft for the MOOee (OEM) flight shape as predicted by a steady RANS simulation with free transition modeling. The results in terms of the location of the transition line along the span of the wing are very close to the design flight shape, parts of the wing near the kink and at the tip even show larger areas of laminar flow. The results for the largest structural deformations, corresponding to the MTOAa (MTOM) mass case, are shown in Figure 13. The skin friction coefficient as well as the location of the transition line along the span for this mass case is very close to the one from the empty mass case (Figure 12), the differences are marginal even though the bending deformations show a difference of approximately 3% with respect to the semi-span of the wing (as represented in Figure 9). The similar flow patterns are essentially the result of similar twist distributions (Figure 9) with only small differences in the outer regions of the wing of approximately 0.2 degrees. The results of all four mass cases and the original flight shape are plotted in Figure 14. These results reveal that, despite the different structural shapes caused by the different mass cases, the aerodynamic characteristics of the laminar wing of the DLR HARW aircraft are – to a certain extend – rather unaffected by structural deformations. For now, additional constraints or an extension of the objective function for the structural optimization with the goal to modify the stiffness properties of the wing are not necessary at this point. The pressure coefficient of the right wing is shown in Figure 15 for the MTOAa (MTOM) mass case. It shows a very homogeneous distribution along the span of the wing with favorable pressure gradient from the leading edge to the shock.

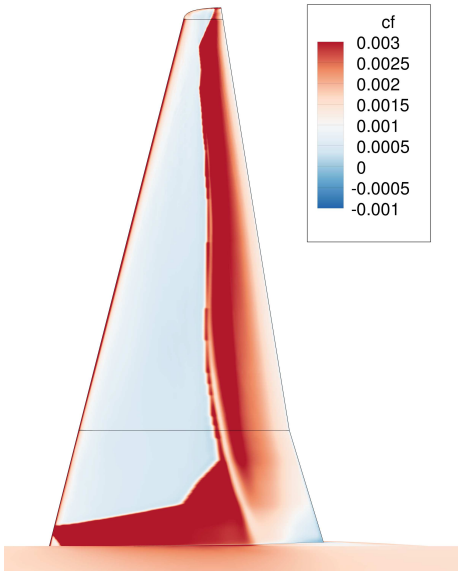

Figure 12 – Skin friction coefficient on the upper surface of the right wing of the DLR HARW aircraft for the MOOee (OEM) flight shape as predicted by steady RANS simulation with free transition modeling.

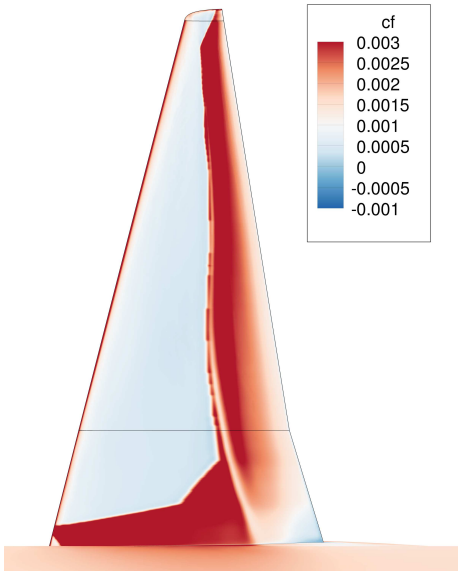

Figure 13 – Skin friction coefficient on the upper surface of the right wing of the DLR HARW aircraft for the MTOAa (MTOM) flight shape as predicted by steady RANS simulation with free transition modeling.

4. Conclusion and Outlook

The structural optimization process and steady RANS CFD analyses of a mid-range jet transport aircraft with CATNLF wing technology have been presented in this work. The goal was to work out if the stiffness properties of the structural model must be modified (increased) during the structural optimization process to account for the particular, probably more sensible nature of the laminar wing to structural deformations. To this end, the structural model was first optimized using a set of steady maneuver and unsteady gust load cases according to the EASA CS-25 specifications. Five different mass cases have been taken into account, ranging from OEW up to MTOW. To assess the sensitivity of the laminar wing with respect to structural deformations, caused by different payload and fuel combinations as reflected by the different mass cases, the structural deformations in 1g steady straight horizontal flight from four selected mass cases have been used. These structural deformations have been interpolated onto a CFD grid. The CFD simulations include the modeling of the free transition of

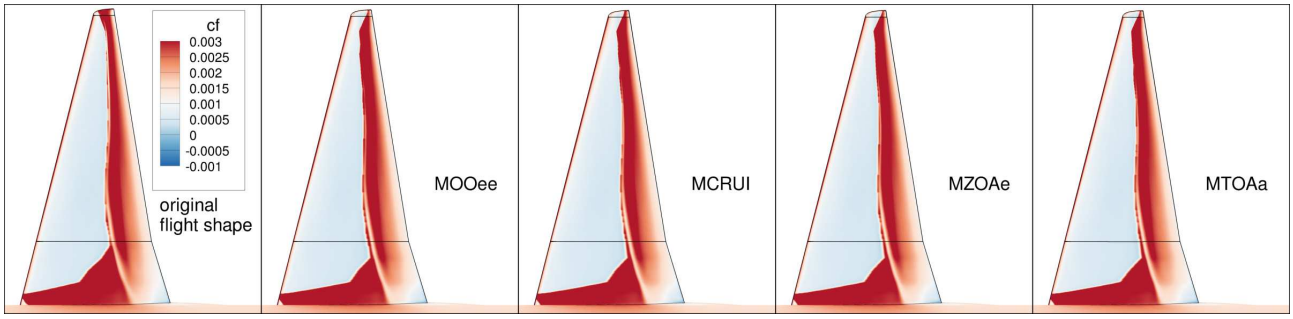

Figure 14 – Skin friction coefficients on the upper surface of the right wing of the DLR HARW aircraft for the original flight shape and all four mass cases as predicted by steady RANS simulation with free transition modeling.

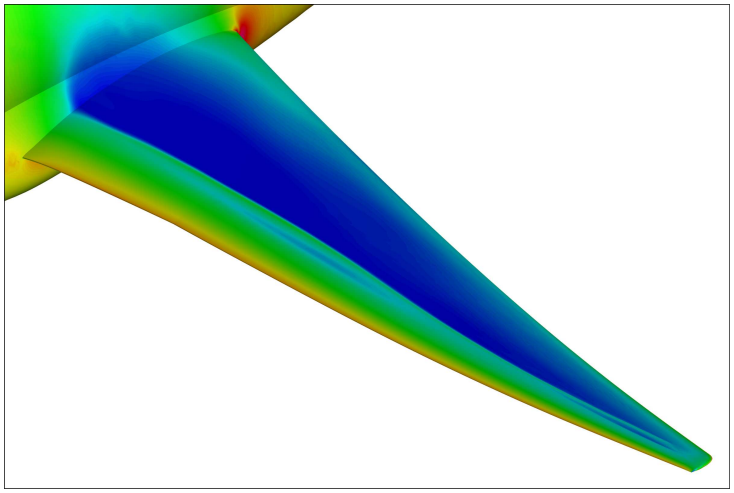

Figure 15 – Pressure coefficient distribution on the upper surface of the right wing of the DLR HARW aircraft for the MTOAa (MTOM) flight shape.

the flow and thus enable a comprehensive evaluation of the impact of the structural deformations on the flow characteristics. The results reveal that the laminar wing of the DLR HARW aircraft is robust in terms of the structural deformations caused by the four mass cases. Thus additional constraints or objectives regarding the stiffness of the wing in the optimization of the structural model can be omitted.

5. Acknowledgements

The authors would like to thank Javier Ruberte Bailo and Thomas Streit from the DLR Institute of Aerodynamics and Flow Technology for the design and provision of the NLF wing shape and the generation of the initial CAD model of the aircraft. The support from Matthias Schulze of the DLR Institute of Aeroelasticity for cpacs-MONA is acknowledged. Furthermore, the support of Alexander Büscher from Airbus Operations GmbH for the aerodynamic design of the wing is acknowledged.
This work was performed within the German LuFo project ULTIMATE: Ultra high efficient wing and moveables for next generation aircraft. LuFo is the national German Aeronautical Research Program. The LuFo project ULTIMATE is a research collaboration between Airbus, DLR, ETW, Liebherr, Technical University Berlin and the Technical University Hamburg. The authors thank the Federal Ministry for Economic Affairs and Climate Action (Bundesministerium für Wirtschaft und Klimaschutz - BMWK) for the funding as part of LuFo VI-2 in the project ULTIMATE.

6. Contact Author Email Address

For questions related to the technical aspects of this work please contact: markus.ritter@dlr.de

7. Copyright Statement

References

[1] DLR Institute of Aerodynamics and Flow Technology. Virtual design environment for real, efficient engineering. *https://www.dlr.de/as/en/desktopdefault.aspx/tabid-18287/29084_read-76559*

[2] Schulze, M. et al. The Effect of Aspect Ratio Variation on the Preliminary Aeroelastic Assessment of a Mid-Range Transport Aircraft. *International Forum on Aeroelasticity and Structural Dynamics (IFASD), The Hague, The Netherlands, 2024*

[3] Lynde, M. N. and Campbell, R. L. Computational Design and Analysis of a Transonic Natural Laminar Flow Wing for a Wind Tunnel Model. *35th AIAA Applied Aerodynamics Conference, Denver, Colorado, 2017*

[4] Rivers, M. B. et al. Experimental Investigation of the NASA Common Research Model with a Natural Laminar Flow Wing in the NASA Langley National Transonic Facility. *AIAA Scitech 2019 Forum, San Diego, California, 2019*

[5] Streit, T. et al. NLF Potential of Laminar Transonic Long Range Aircraft. *AIAA Aviation 2020 Forum, USA, Virtual Event*

[6] Streit, T. and Ruberte Bailo, J. and Seitz, A. Design of a Highly Efficient Transport NLF Aircraft with a Backward Swept Wing and a Long Single-Aisle Fuselage. *34th International Council of the Aeronautical Sciences (ICAS), Florence, Italy, 2024*

[7] Schulze, M. and Neumann, J. and Klimmek, T. Parametric Modeling of a Long-Range Aircraft under Consideration of Engine-Wing Integration. *MDPI Aerospace 2021, 8 (1), https://www.mdpi.com/2226-4310/8/1/2*

[8] Klimmek, T. et al. cpacs-MONA – An Independent and in High-Fidelity Based MDO Tasks Integrated Process for the Structural and Aeroelastic Design of Aircraft Configurations. *International Forum on Aeroelasticity and Structural Dynamics (IFASD), Savannah, USA, 2019*

[9] Klimmek, T. and Schulze, M. and Wöhler, S. Investigation on Aeroelastic Characteristics due to Structural and Geometrical Variations for an SMR Aircraft Configuration using cpacsMONA. *Deutscher Luft- und Raumfahrt Kongress (DLRK), Stuttgart, Germany, 2023*

[10] Sinha, K. et al. Loads analysis and structural optimization of a high aspect ratio composite wing aircraft. *Springer CEAS Aeronautical Journal, Vol. 12, pp. 233-243, 2021*

[11] Abu-Zurayk, M. et al. Comparing Two Multidisciplinary Optimization Formulations of Trimmed Aircraft Subject to Industry-relevant Loads and Constraints *AIAA AVIATION Forum, Washington DC, USA, 2021*

[12] Alder, M. et al. Recent Advances in Establishing a Common Language for Aircraft Design with CPACS. *Aerospace Europe Conference, Bordeaux, France, 2020*

[13] DLR. The Common Parametric Aircraft Configuration Schema (CPACS). *https://dlr-sl.github.io/cpacs-website*

[14] Pinho Chiozzotto, G. Improving aircraft conceptual design with methods for wing loads, aeroelasticity and mass estimation. *Dissertation, Technische Universität Berlin, 2019*

[15] van Dalen, F. MDO load analysis and preliminary sizing. *Delft University of Technology, Delft, Netherlands, 1996*

[16] Guyan, R. J. Reduction of Stiffness and Mass Matrices. *AIAA Journal, Vol. 3, p. 380, 1964*

[17] European Union Aviation Safety Agency (EASA). CS-25 Large Aeroplanes Certification Specifications

[18] Schwamborn, D. and Gerhold, T. and Heinrich, R. The DLR TAU-Code: Recent Applications in Research and Industry. *ECCOMAS 2006, Delft, 2006*

[19] Schrauf, G. COCO - A Program to Compute Velocity and Temperature Profiles for Local and Nonlocal Stability Analysis of Compressible, Conical Boundary Layers with Suction. *ZARM Technik Report, 1998*

[20] Krumbein, A. and Krimmelbein, N. and Schrauf, G. Automatic Transition Prediction in Hybrid Flow Solver, Part 1: Methodology and Sensitivities. *Journal of Aircraft", Vol. 46, No. 4, pp. 1176–1190, 2009*

[21] Krumbein, A. and Krimmelbein, N. and Schrauf, G. Automatic Transition Prediction in Hybrid Flow Solver, Part 2: Practical Application. *Journal of Aircraft, Vol. 46, No. 4, pp. 1191–1199, 2009*

[22] Smith, A. M. O. and Gamberoni, N. Transition, Pressure Gradient and Stability Theory. *Douglas Aircraft Co. Report ES 26388, 1956*

[23] van Ingen, J. L. A Suggested Semi-Empirical Method for the Calculation of the Boundary Layer Transition Region. *Department of Aerospace Engineering, University of Delft, The Netherlands, Report VTH-74, 1956*